Acta Crystallographica Section D
Biological Crystallography
ISSN 0907-4449

The effect of a proline residue on the rate of growth and the space group of α-spectrin SH3-domain crystals

Ana Cámara-Artigas,[a]* Monserrat Andújar-Sánchez,[a] Emilia Ortiz-Salmerón,[a] Celia Cuadri[a] and Salvador Casares[b]

[a]Departamento Química-Física, Bioquímica y Química Inorgánica, Universidad de Almería, Carretera Sacramento, Almería 04120, Spain, and [b]Departamento Química-Física, Universidad de Granada, Avenida Fuentenueva s/n, Granada 18002, Spain

Correspondence e-mail: acamara@ual.es

Received 13 July 2009
Accepted 20 September 2009

PDB Reference: GDS mutant α-spectrin SH3 domain, 3i9q, r3i9qsf.

α-Spectrin SH3-domain (Spc-SH3) crystallization is characterized by very fast growth of the crystals in the presence of ammonium sulfate as a precipitant agent. The origin of this behaviour can be attributed to the presence of a proline residue that participates in a crystal contact mimicking the binding of proline-rich sequences to SH3 domains. This residue, Pro20, is located in the RT loop and is the main contact in one of the interfaces present in the orthorhombic Spc-SH3 crystal structures. In order to understand the molecular interactions that are responsible for the very fast crystal growth of the wild-type (WT) Spc-SH3 crystals, the crystal structure of a triple mutant in which the residues Ser19-Pro20-Arg21 in the RT loop have been replaced by Gly19-Asp20-Ser21 (GDS Spc-SH3 mutant) has been solved. The removal of the critical proline residue results in slower nucleation of the Spc-SH3 crystals and a different arrangement of the protein molecules in the unit cell, leading to a crystal that belongs to the tetragonal space group $P4_12_12$, with unit-cell parameters $a = b = 42.231$, $c = 93.655$ Å, and that diffracts to 1.45 Å resolution. For both WT Spc-SH3 and the GDS mutant, light-scattering experiments showed that a dimer was formed in solution within a few minutes of the addition of 2 *M* ammonium sulfate at pH 6.5 and allowed the proposal of a mechanism for the nucleation and crystal growth of Spc-SH3 in which the Pro20 residue plays a key role in the rate of crystal growth.

1. Introduction

The Src-homology region 3 (SH3) domain is one of the most widely found modular domains in all eukaryotic genomes. These domains have also become a very important focus of interest in rational drug design since they are involved in transient protein–protein interactions that are related to a large number of cell processes, many of them connected to pathological conditions (Kay *et al.*, 2000; Gmeiner & Horita, 2001; Mayer & Saksela, 2004). This small globular protein consists of two orthogonal β-sheets, each of which is formed by three antiparallel β-strands. The loops connecting strands β1–β2, β3–β4 and β5–β6 are named the RT, n-Src and distal loops, respectively. SH3 domains interact with proline-rich sequences with a consensus conserved P*xx*P binding motif, adopting the polyproline II (PPII) helical conformation. The binding interface of the SH3 domains is outlined by a hydrophobic surface that is located between the RT loop and the n-Src loop and that contains three shallow pockets defined by conserved aromatic residues. Two of the pockets accommodate the prolines in the P*xx*P motif and the third pocket, which is known as the 'specificity pocket', plays a crucial role in both the affinity and the specificity of the interaction.

The first structure of the chicken α-spectrin SH3 domain (Spc-SH3) was solved by Musacchio *et al.* (1992). Since then, the structures of more than 20 different Spc-SH3 variants have been solved by means of X-ray crystallography (Musacchio *et al.*, 1992; Vega *et al.*, 2000; Berisio *et al.*, 2001; Casares *et al.*, 2007) and NMR (Casares *et al.*, 2007). All of the solved crystallographic structures of Spc-SH3 variants belong to the orthorhombic space group $P2_12_12_1$ with approximately the same unit-cell parameters, with the exception of the structures of chimeras or circular permutants (Viguera *et al.*, 1995; Gushchina *et al.*, 2009). A very interesting and striking feature of these orthorhombic crystals is the remarkably fast growth observed in the presence of ammonium sulfate. To date, the basis of this rapid growth has not been established. One of the two interfaces present in the crystal structures of Spc-SH3 has a single contact provided by Pro20. Hydrophobic contacts are involved in physiological protein–protein interactions, but these types of contacts are not usually found at protein crystal interfaces (Dasgupta *et al.*, 1997). In order to elucidate the role of Pro20 in the growth rate of the crystal, we have crystallized a mutant variant of Spc-SH3 in which three of the residues of the RT loop have been replaced (Ser19Gly, Pro20Asp and Arg21Ser) and the crystal structure of this triple mutant (GDS Spc-SH3) has been solved at 1.45 Å resolution.

2. Materials and methods

2.1. Protein purification and crystallization of the triple mutant

To investigate the role of the Pro20 residue in the crystallization mechanism of Spc-SH3, a triple mutant (GDS Spc-SH3) was designed to remove the proline residue from the RT loop while maintaining the stability of the protein. In this mutant, residues Ser19, Pro20 and Arg21 were replaced by Gly, Asp and Ser, respectively. The protein was cloned and overexpressed from a pET-type plasmid in *Escherichia coli* strain BL21 (DE3). Cultured cells were collected by centrifugation and lysed in 5.0 m*M* sodium citrate pH 3.5 using a French press. The protein was found to be soluble under mildly acidic conditions and thus the pH of the cell lysate was lowered to 3.0. Most of the cell's proteins precipitated while GDS Spc-SH3 remained soluble. The acidified lysate was clarified by ultracentrifugation and the protein was recovered from the supernatant by precipitation in 75% saturation ammonium sulfate. Precipitated protein was solubilized in 50.0 m*M* sodium phosphate buffer and 100 m*M* NaCl pH 7.0 containing 6.0 *M* urea and further dialyzed against the same buffer. The protein was finally purified by size-exclusion chromatography on a HiLoad Superdex 75 column (GE Healthcare). SDS–PAGE was used as a test to assure protein purity. Protein aliquots were extensively dialyzed against deionized water and further lyophilized. For crystallization experiments, lyophilized protein was dissolved directly in 5.0 m*M* glycine pH 3.0 buffer and the concentration was determined spectrophotometrically as described previously (Casares *et al.*, 2007).

Table 1
Data-collection and refinement statistics.

Values in parentheses are for the highest resolution bin.

Space group	$P4_12_12$
Unit-cell parameters (Å, °)	$a = b = 42.231$, $c = 93.655$, $\alpha = \beta = \gamma = 90.00$
Resolution range (Å)	20–1.45
No. of observations	202864
Unique reflections	15182 (1552)
Redundancy	13.4 (13.9)
Data completeness (%)	95.8 (99.9)
$R_{\rm merge}$† (%)	6.30 (43.3)
Average $I/\sigma(I)$	28.89 (6.82)
Refinement	
Protein residues	56
Solvent	59
$R_{\rm work}$ (%)	23.2 (35.7)
$R_{\rm free}$ (%)	24.3 (45.2)
R.m.s. deviations from ideal geometry	
Bonds (Å)	0.018
Angles (°)	2.371
Mean B (protein) (Å^2)	14.17
Residues in allowed regions of the Ramachandran plot‡ (%)	98.2

† $R_{\rm merge} = \sum_{hkl}\sum_i |I_i(hkl) - \langle I(hkl)\rangle| / \sum_{hkl}\sum_i I_i(hkl) \times 100$, where $\langle I(hkl)\rangle$ is the mean intensity of i reflections with intensity $I_i(hkl)$. ‡ From *PROCHECK* statistics.

2.2. Crystallization and data collection.

As a standard crystallization procedure, 6 µl drops were prepared by mixing 3 µl protein solution at 5 mg ml^{-1} with 3 µl of a precipitant solution composed of 2 *M* ammonium sulfate and 0.1 *M* MES pH 6.5. The protein drop was allowed to equilibrate against 1 ml precipitant solution at 298 K. As a control, drops of the WT protein were placed in the same Linbro plate using the same crystallization conditions and photographs were taken of both samples during the crystal-growth process.

For data collection, the crystals were soaked in a cryoprotectant solution containing 10% glycerol, 2 *M* ammonium sulfate and 0.1 *M* MES pH 6.5, looped and placed in a cold nitrogen stream maintained at 110 K. X-ray diffraction data collection was performed at the beamline BM-16 station of the European Synchrotron Radiation Facility (ESRF) using a MAR CCD 165 detector at a wavelength of 0.97 Å. Data were indexed, integrated and scaled with the *HKL*-2000 suite (Otwinowski & Minor, 1997). The resulting crystallographic parameters and statistics of data collection are listed in Table 1.

2.3. Structure solution and refinement.

The structure of the GDS Spc-SH3 mutant was solved by molecular replacement using *MOLREP* (Vagin & Teplyakov, 1997). The crystal belonged to space group $P4_12_12$ or $P4_32_12$ and the molecular-replacement procedure was conducted in both space groups to solve the ambiguity. The coordinates of WT Spc-SH3 (PDB entry 1shg) were used as a search model (Musacchio *et al.*, 1992). A translation function calculated for space group $P4_12_12$ gave a clear solution with an R factor of 0.46 after rigid-body refinement. The structure was refined using *REFMAC* v.5.0 (Murshudov *et al.*, 1997). Several cycles of positional refinement and temperature-factor refinement

were alternated with manual building in *Coot* (Emsley & Cowtan, 2004) using σ_A-weighted ($2F_o - F_c$) and ($F_o - F_c$) electron-density maps. Water molecules were placed in the electron-density difference maps using *Coot*. The atomic coordinates of GDS Spc-SH3 have been deposited in the PDB with accession code 3i9q. Superposition and calculation of the r.m.s. deviations of the structures were accomplished using the *CCP*4 program *LSQKAB* (Kabsch, 1976). Finally, a stereochemical analysis of the refined structure was performed with *PROCHECK* (Laskowski *et al.*, 1993). The final refinement statistics are presented in Table 1.

Protein interfaces in the crystals were characterized using the *PISA* server (Krissinel & Henrick, 2005). Distances between amino acids were calculated using *CONTACT* from the *CCP*4 suite (Collaborative Computational Project, Number 4, 1994).

2.4. Dynamic and static light-scattering experiments

Dynamic light-scattering (DLS) and static light-scattering (SLS) measurements were performed with a Zetasizer Nano ZS (Malvern Instruments Ltd) using a thermostatized 30 µl quartz sample cuvette. Samples of Spc-SH3 were prepared at different concentrations (1–10 mg ml^{-1}) in 0.1 *M* MES pH 6.5. Measurements were conducted with the protein solution alone and in the presence of 1 *M* ammonium sulfate. All solutions were filtered and protein samples were centrifuged for 30 min at 14 000 rev min^{-1} immediately before measurement in order to remove any aggregates and dust. DLS measurements were performed on each sample at 298 K to determine the hydrodynamic radius (R_h). The molecular mass of the molecules present in the solution was determined using a Debye plot, which allows the determination of both the absolute molecular mass and the second virial coefficient (A_2). Data were analyzed using the software developed by Malvern Instruments Ltd.

3. Results

3.1. GDS Spc-SH3 crystal growth

Spc-SH3 crystals grow from solutions containing ammonium sulfate as a precipitant agent under a broad range of pH conditions (4–9), but the most interesting feature of these crystals is how rapidly they grow even at moderate protein concentrations: WT Spc-SH3 crystals appeared only 1 min after mixing the protein at 5 mg ml^{-1} with 2 *M* ammonium sulfate, 0.1 *M* MES buffer pH 6.5 and it took only 1 h to fully grow all crystals in the drop. However, for the triple mutant GDS Spc-SH3 the crystals took more than one month to emerge under the same crystallization conditions. Moreover, the WT crystals clearly displayed the long needle shape typical of the orthorhombic space group $P2_12_12_1$, whereas the GDS Spc-SH3 mutant crystals were prism-shaped (Fig. 1). Interestingly, some subtle changes in the GDS Spc-SH3 solution were visible using a microscope just a few minutes after mixing with the precipitant solution. In order to characterize these changes, DLS measurements were performed both in the absence and the presence of precipitant. In the absence of precipitant, both protein variants, WT and GDS Spc-SH3, showed a single population in solution with a hydrodynamic radius (R_h) ranging from 1.6 to 1.8 nm at all protein concentrations tested (1–10 mg ml^{-1}). These values are comparable to those reported in previous studies of WT Spc-SH3 as well as for other SH3 domains (Camara-Artigas *et al.*, 2009) which remain monomeric even at very high protein concentrations. A Debye plot of the SLS measurements of GDS Spc-SH3 yielded a molecular mass of 6 kDa, which is close to the value of 7 kDa calculated from its sequence. In contrast, upon the addition of 1 *M* ammonium sulfate to GDS Spc-SH3 solution DLS experiments showed a single peak corresponding to an R_h value of 2.8–2.9 nm. In this case the linear fitting of the Debye plot yields a negative slope with a second virial coefficient (A_2) of -7×10^{-4} mol ml^{-1} g^{-2} and a molecular mass of 13 kDa. These results indicate that the only significantly populated species under these conditions is a dimer. The formation of the dimer is a relatively quick process that is completed within a few minutes of the addition of precipitant. Interestingly enough, the hydrodynamic radius did not change upon extended incubation at 298 K up to the actual appearance of crystals.

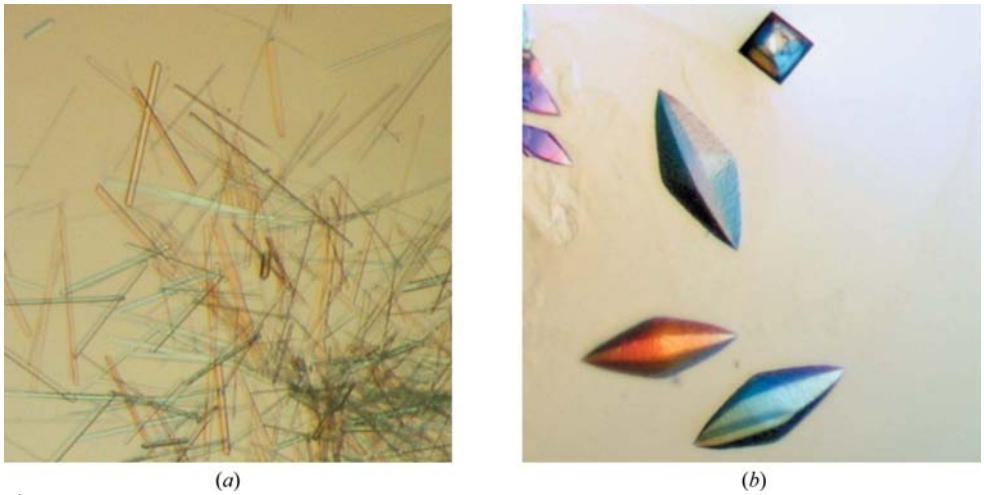

Figure 1
(*a*) WT Spc-SH3 and (*b*) GDS Spc-SH3 mutant crystals. The crystals were grown by mixing 5 µl protein solution at 10 mg ml^{-1} with 5 µl precipitant solution (2 *M* ammonium sulfate in 0.1 *M* MES pH 6.5) and the drops were equilibrated against 1 ml precipitant solution using a hanging-drop setup.

3.2. GDS Spc-SH3 structure

The rate of crystal growth is not the only difference observed between the WT and GDS Spc-SH3 crystals. The molecular-replacement solution showed that the mutant crystals belong to the tetragonal space group $P4_12_12$

and the asymmetric unit consists of just one polypeptide chain with a Matthews coefficient of 2.99 Å^3 Da^{-1} (58.93% solvent content). The high quality of the data collected allowed us to model 56 out of a total of 62 residues. The amino-terminal region of Spc-SH3 is very flexible and thus the full-length Spc-SH3 structure has only been determined for the A65G Spc-SH3 mutant (Casares *et al.*, 2007), in which an unusually tight packing restrains the flexibility of the chain (the Matthews coefficient of the A65G Spc-SH3 mutant crystal is 1.64 Å^3 Da^{-1} and its solvent content is 25.11%). The overall three-dimensional structure is the same as those reported for the WT and other Spc-SH3 variants and consists of a single β-barrel hydrophobic core formed by two perpendicular three-stranded β-sheets, where only Asn47 is found to be outside the allowed regions of the Ramachandran plot. This residue is located at the tip of the distal β-turn, which is formed by the residues Val46-Asn47-Asp48-Arg49, and exhibits a slightly different conformation in each of the crystal structures deposited in the PDB. This variability in the distal β-turn conformation might be related to the intrinsic low stability of the loop (Martinez & Serrano, 1999; Morel *et al.*, 2006). The availability for the first time of a different crystal form allowed us to investigate the effect of crystal packing on the distal-loop conformation of Spc-SH3. The r.m.s.d. plot shows that the main differences in the backbone position between the GDS Spc-SH3 mutant and all other Spc-SH3 structures are primarily located in this loop. Interestingly, apart from the triple mutant, the r.m.s.d. values in the RT loop among different structures are smaller than the values obtained for the distal loop. The residues in the RT loop have been proven to play a key role in the folding and stability of Spc-SH3 (Casares *et al.*, 2007) and we used a triple mutant instead of the single Pro20 mutant in order to retain the same stability as for WT Spc-SH3. Following this rationale, we decided to apply sequence modifications to the RT loop of Spc-SH3 in order to mimic the sequence of the homologous loop in Abl-SH3, which does not contain proline, and finally the triple mutant GDS resulted in the expected unchanged stability. In fact, the triple mutant shows a thermodynamic stability that is comparable to that of the WT variant as measured by differential scanning calorimetry (DSC): at pH 7, the T_m and ΔG_U values are 336.7 K and 16.0 kJ mol^{-1} for the WT, and 334.7 K and 18.4 kJ mol^{-1} for the triple-mutant protein (unpublished data). There are not large differences in the backbone atoms of the RT loop, as shown by the r.m.s.d. values obtained, but the side chains of the triple mutant show higher *B* factors than the average values for the entire structure. This indicates that the side chains at the engineered RT loop show higher mobility than their counterparts in the WT form. On the other hand, the *B*-factor values for the side

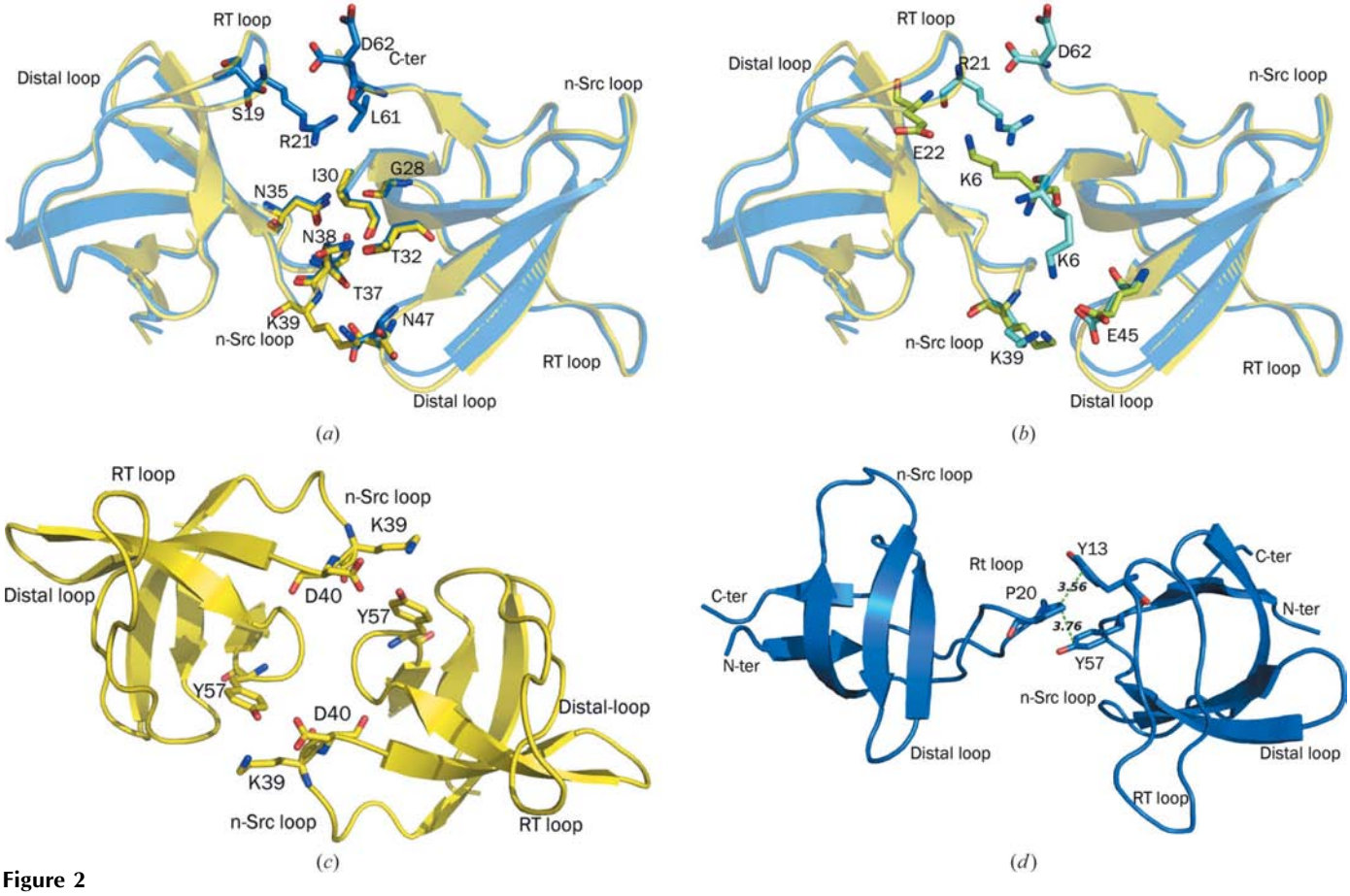

Figure 2
(*a*) Hydrogen bonds and (*b*) salt bridges present at interface 1 of WT Spc-SH3 (blue) and GDS Spc-SH3 (yellow). Details of interface 2 of WT Spc-SH3 and GDS Spc-SH3 are shown in (*c*) and (*d*), respectively.

chains are comparable to those of residues located in the RT loop of Abl-SH3 structures. The increase in mobility of the side chains has also been observed in structures of the R21D mutant of Spc-SH3, where this observation was made for crystals obtained at basic pH values (pH > 7) but not for those obtained at acidic pH values. Remarkably, this increase in the mobility of the side chains does not affect the rate of crystal growth, which remains the same as that observed for the WT protein (data not shown).

3.3. GDS Spc-SH3 crystal contacts and packing

To study how the crystal packing affects the conformation of the loop as well as the contacts established in the orthorhombic and tetragonal crystal forms, we analyzed the crystal interfaces of all Spc-SH3 structures using the *PISA* web server (Krissinel & Henrick, 2005). When the crystal interfaces of GDS Spc-SH3 were analyzed, the first interface was found to be equivalent to that found in the orthorhombic structures and shares the same hydrogen-bonding and salt-bridge network, with the only exception being the salt bridge formed by Arg21 and Asp62 (Fig. 2). The Arg21 residue has been mutated to serine in the GDS Spc-SH3 mutant and serine is not capable of forming salt bridges. However, a glutamate residue is located next to this serine and thus a new salt bridge can be established between Glu22 and Lys6 (distance of ∼2.5 Å). The same type of salt bridge is observed in the Arg21 mutant structures, where the positive-charged amino acid has been replaced by either uncharged or negatively charged residues (Casares *et al.*, 2007; Camara-Artigas *et al.*, in preparation). For example, in the WT Spc-SH3 structure the distance between Lys6 and Glu22 is greater than 10 Å owing to the repulsive interaction between Arg21 and Lys6. Formation of the salt bridge requires that Lys6 changes its spatial orientation towards the RT loop of the symmetry-related molecule. This arrangement brings the Lys6 and Glu22 residues together to a suitable distance for the salt bridge to be established. This is the most significant change observed in the first interface of the GDS Spc-SH3 mutant when compared with those of other Spc-SH3 structures. In general, this interface is a clear example of nonspecific interactions that take place *via* hydrogen bonds, ionic and van der Waals contacts.

The second interface of the GDS Spc-SH3 differs from that observed in the orthorhombic structures. Fig. 2 shows this interface, in which the contacts are stabilized by hydrogen bonds between Lys39 and Tyr57 and between Asp40 and Tyr57. A third interface can be found in this crystal form in which residue Asp48 participates in a hydrogen bond to the backbone N atom of Asp14 of the symmetry-related molecule. This contact may explain why the major differences found in the r.m.s.d. values of the triple mutant compared with those of other Spc-SH3 structures are primarily localized in this loop. In addition, the electronic density of the residues at the distal loop is much better defined than that found in other SH3 structures where this loop does not participate in the crystal contacts.

4. Discussion

When we crystallized the triple mutant GDS Spc-SH3, which lacks the Pro20 residue, a drastic decrease in the rate of the crystal growth was observed compared with that for WT Spc-SH3. Pro20 participates in the only contact present at the second interface of the orthorhombic crystal form. Fig. 2 shows the Pro20–Tyr13–Tyr57 contact, which is indeed quite similar to that formed by the first proline in the P*xx*P binding motif. If the contact of Pro20 with the symmetry-related Tyr13–Tyr57 pocket is comparable to those established in the complex structures of SH3 domains with their partner peptide ligands, then similar behaviour can be expected. This means that this contact is favoured by the burial of hydrophobic surface at a reasonably low entropic cost from a thermodynamic point of view and moreover that the rate of formation of such contacts might be comparable to the value of the kinetic rate of formation of this contact in the SH3–peptide complex. This kinetic rate constant has been measured for the binding of proline-rich motifs to SH3 domains and values of the order of magnitude of $10^8\ M^{-1}\ s^{-1}$ have been reported (Demers & Mittermaier, 2009). Also, these rate constants do not vary significantly over a broad temperature range, implying that the association of the SH3 domain with its peptide ligand does not entail a large enthalpic barrier. Indeed, the value of this association rate constant is of the same order of magnitude as those reported for other protein–ligand interactions that have been proposed to be diffusion-limited (Gabdoulline & Wade, 2002). As a result, a high protein concentration is not required to reach the critical nucleus and the subsequent growth of the crystals under specific supersaturation conditions (McPherson, 1999; García-

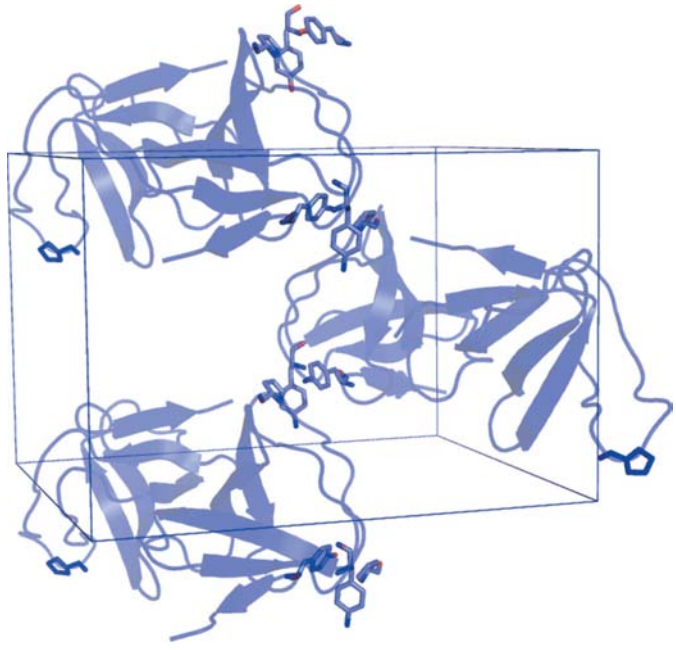

Figure 3
Packing of the orthorhombic crystal form. The dimer is formed in solution and it can be considered to be the building block of the crystal, which then grows through the contact formed by the Pro20 and Tyr13–Tyr57 contacts (sticks).

Ruiz, 2003) because this specific contact favours the rapid assembly of protein units to build up the crystal. The specific nature of this contact can be also deduced from the values of the parameters obtained for the interface using the *PISA* server (Krissinel & Henrick, 2007). Indeed, the second interface of the WT Spc-SH3 structure has a P $\Delta^i G$ value of 0.265 and a $\Delta^i G$ value of $-11.3\ \mathrm{kJ\ mol^{-1}}$. The negative $\Delta^i G$ confirms the burial of hydrophobic interfaces and the low P value suggests that these hidden interfaces have a much higher hydrophobicity than expected, which implies that the contact present at this interface might be the result of a specific interaction.

Despite the differences in crystal packing and unit-cell parameters, the major interface is comparable between all the orthorhombic Spc-SH3 and GDS Spc-SH3 structures. The shared character of the first interface led us to propose that the dimer including this interface operates as a prenucleation aggregate in crystal growth. We have confirmed the presence of this dimer in the crystallization solution prior to actual crystal formation by light-scattering studies. The formation of prenucleation aggregates as crystal building blocks has previously been proposed for proteins (Kadima *et al.*, 1990). Once the dimer has been formed, the Pro20 contact in the second interface of the orthorhombic structures promotes fast growth of these crystals, which starts only a few minutes after the addition of the precipitant solution to the protein.

Here, we have proposed a crystallization mechanism for Spc-SH3 that is compatible with the observations described, in which the first step is the self-association of the monomeric SH3 domains to form dimers *via* electrostatic interactions. The ammonium and sulfate ions in solution compete for the solvation of the charged residues at the surface of the protein, favouring their burial. Electrostatic interactions play a decisive role in the diffusional association (Gabdoulline & Wade, 2002) and thus can affect the rate of crystal growth. However, many other forces may modulate this mechanism. Camacho and coworkers demonstrated that hydrophobic desolvation can be extremely important for electrostatically weakly attracting proteins (Camacho *et al.*, 2000). Once the mainly charged surface of the protein is buried in the dimer, only a few charged residues remain exposed. Pro20 facilitates growth of the dimers in a three-dimensional manner by desolvation of the hydrophobic Pro20 and Tyr13–Tyr57 residues (Fig. 3). This hydrophobic contact changes the dynamics of the association events favouring the formation of the critical nucleus and thus accelerates crystal growth.

This research was funded by grants BIO2006-15517-C02-01 and BIO2006-15517-C02-02 from the Spanish Ministry of Education and Sciences and grants to the research groups BIO-292 from the Andalusian Regional Government. We would also like to thank the Project 'Factoría Española de Cristalización' for data collection.

References

Berisio, R., Viguera, A., Serrano, L. & Wilmanns, M. (2001). *Acta Cryst.* D**57**, 337–340.
Camacho, C. J., Kimura, S. R., DeLisi, C. & Vajda, S. (2000). *Biophys. J.* **78**, 1094–1105.
Camara-Artigas, A., Martín-García, J. M., Morel, B., Ruiz-Sanz, J. & Luque, I. (2009). *FEBS Lett.* **583**, 749–753.
Casares, S., Ab, E., Eshuis, H., Lopez-Mayorga, O., van Nuland, N. A. & Conejero-Lara, F. (2007). *BMC Struct. Biol.* **7**, 22.
Casares, S., López-Mayorga, O., Vega, M. C., Cámara-Artigas, A. & Conejero-Lara, F. (2007). *Proteins*, **67**, 531–547.
Collaborative Computational Project, Number 4 (1994). *Acta Cryst.* D**50**, 760–763.
Dasgupta, S., Iyer, G. H., Bryant, S. H., Lawrence, C. E. & Bell, J. A. (1997). *Proteins*, **28**, 494–514.
Demers, J. P. & Mittermaier, A. (2009). *J. Am. Chem. Soc.* **131**, 4355–4367.
Emsley, P. & Cowtan, K. (2004). *Acta Cryst.* D**60**, 2126–2132.
Gabdoulline, R. R. & Wade, R. C. (2002). *Curr. Opin. Struct. Biol.* **12**, 204–213.
García-Ruiz, J. M. (2003). *Methods Enzymol.* **368**, 130–154.
Gmeiner, W. H. & Horita, D. A. (2001). *Cell Biochem. Biophys.* **35**, 127–140.
Gushchina, L. V., Gabdulkhakov, A. G., Nikonov, S. V., Mateo, P. L. & Filimonov, V. V. (2009). *Biophys. Chem.* **139**, 106–115.
Kabsch, W. (1976). *Acta Cryst.* A**32**, 922–923.
Kadima, W., McPherson, A., Dunn, M. F. & Jurnak, F. A. (1990). *Biophys. J.* **57**, 125–132.
Kay, B. K., Williamson, M. P. & Sudol, M. (2000). *FASEB J.* **14**, 231–241.
Krissinel, E. & Henrick, K. (2005). *CompLife 2005*, edited by M. R. Berthold, R. Glen, K. Diederichs, O. Kohlbacher & I. Fischer, pp. 163–174. Berlin/Heidelberg: Springer-Verlag.
Krissinel, E. & Henrick, K. (2007). *J. Mol. Biol.* **372**, 774–797.
Laskowski, R. A., MacArthur, M. W., Moss, D. S. & Thornton, J. M. (1993). *J. Appl. Cryst.* **26**, 283–291.
Martinez, J. C. & Serrano, L. (1999). *Nature Struct. Biol.* **6**, 1010–1016.
Mayer, B. J. & Saksela, K. (2004). *Modular Protein Domains*, edited by G. Cesareni, M. Gimona, M. Sudol & M. Yaffe, pp. 37–55. Weinheim: Wiley-VCH.
McPherson, A. (1999). *Crystallization of Biological Macromolecules.* New York: Cold Spring Harbor Laboratory Press.
Morel, B., Casares, S. & Conejero-Lara, F. (2006). *J. Mol. Biol.* **356**, 453–468.
Murshudov, G. N., Vagin, A. A. & Dodson, E. J. (1997). *Acta Cryst.* D**53**, 240–255.
Musacchio, A., Noble, M., Pauptit, R., Wierenga, R. & Saraste, M. (1992). *Nature (London)*, **359**, 851–855.
Otwinowski, Z. & Minor, W. (1997). *Methods Enzymol.* **276**, 307–326.
Vagin, A. & Teplyakov, A. (1997). *J. Appl. Cryst.* **30**, 1022–1025.
Vega, M. C., Martínez, J. C. & Serrano, L. (2000). *Protein Sci.* **9**, 2322–2328.
Viguera, A. R., Blanco, F. J. & Serrano, L. (1995). *J. Mol. Biol.* **247**, 670–681.